Available online at www.sciencedirect.com
ScienceDirect
Journal of the European Ceramic Society 31 (2011) 3021–3031
www.elsevier.com/locate/jeurceramsoc

# Matrix–filler interactions in polysilazane-derived ceramics with $Al_2O_3$ and $ZrO_2$ fillers

Thomas Konegger[a,*], Robert Potzmann[b], Michael Puchberger[b], Antje Liersch[a,c]

[a] Institute of Chemical Technologies and Analytics, Vienna University of Technology, Getreidemarkt 9/164-CT, 1060 Vienna, Austria
[b] Institute of Materials Chemistry, Vienna University of Technology, Getreidemarkt 9/165, 1060 Vienna, Austria
[c] Department Materials Science, Glass and Ceramics, Koblenz University of Applied Sciences, Rheinstraße 56, 56203 Höhr-Grenzhausen, Germany

Received 7 March 2011; received in revised form 4 July 2011; accepted 10 July 2011
Available online 4 August 2011

**Abstract**

Interactions between a poly(vinyl)silazane and $Al_2O_3$ or $Y_2O_3$-stabilised $ZrO_2$ fillers were studied during the fabrication of polysilazane-derived bulk ceramics in order to investigate the influence of oxide fillers on resulting properties. Specimens were produced by coating of the filler powders with the polysilazane, warm-pressing of the resulting composite powders, and pyrolytic conversion in flowing $N_2$ at various temperatures between 1000 °C and 1400 °C. Significant differences in densification were observed, depending on the filler used. Reactions between the polysilazane-derived matrix and $Al_2O_3$ or $ZrO_2$ at temperatures ≥1300 °C resulted in the formation of $Si_5AlON_7$ or $ZrSiO_4$, respectively. Reactivity in the polysilazane-derived component was a result of $SiO_2$ contamination caused primarily by adsorbed species on the filler particle surface. Knowledge of polysilazane/filler interface processes is found to be decisive for the prediction of properties such as shrinkage and porosity, which heavily influence performance of a material.


*Keywords:* Precursors-organic; $Al_2O_3$; $ZrO_2$; Composites; Polymer-derived ceramic

## 1. Introduction

The production of ceramic materials by the polymer precursor route is an alternative to the conventional powder processing route due to reduced process temperatures, improved machinability in the green state and the ability to manufacture high purity products. Prominent examples of Si-containing polymeric precursors include polycarbosilanes, polysiloxanes and polysilazanes.[1] The use of polysilazanes in particular has been of interest due to the high-temperature stability[2] and creep resistance[3] of the resulting silicon carbonitrides.

During the pyrolytic conversion from the polymer to the ceramic state, the evolution of gaseous species as well as an increase in density of the material can lead to the formation of pores and cracks and thus significantly complicate the production of bulk bodies.[4] A feasible approach to solving this problem is the addition of filler particles to the preceramic polymer, thereby reducing shrinkage of the composite material during pyrolysis.[5,6] Successfully applied filler materials for polysilane- and polysilazane-derived ceramics include non-oxide ceramics such as SiC,[5] $Si_3N_4$ [6] and cBN[7] or oxide ceramics such as $Al_2O_3$ [8–10] and, more recently, $HfO_2$.[11] SiC and $Si_3N_4$ have been widely regarded as passive fillers, showing little to no reactivity with the polymeric matrix.[12] Passive fillers reduce shrinkage during processing in accordance with filler volume effect.[13] In contrast, active fillers such as metallic or intermetallic powders react with the polysilazane, its decomposition products or with a reactive atmosphere during pyrolytic conversion.[14] An expansion in the filler component during these reactions can be used to counteract shrinkage further and even to lead to near-net shape processing.[13]

One possible way to manufacture polymer-derived ceramics with particulate fillers is the so-called hybrid route, where the filler material is coated with a dissolved polymeric precursor before the mixture is dried, cross-linked, and pyrolytically converted.[8,9] Additionally, combined cross-linking and forming techniques such as warm-pressing can be applied.[10]

* Corresponding author. Tel.: +43 1 58801 16161; fax: +43 1 58801 16199.
*E-mail address:* konegger@mail.tuwien.ac.at (T. Konegger).

0955-2219/$ – see front matter © 2011 Elsevier Ltd. All rights reserved.
doi:10.1016/j.jeurceramsoc.2011.07.015

Contrary to the original classification as passive fillers, reactions between polysilazanes and oxide ceramic fillers such as $Al_2O_3$ during the pyrolytic conversion have been reported in the literature. Oxide ceramic fillers can act as passive or active fillers, depending on the nature of the particles as well as the processing conditions.[15] The combination of a polysilazane with $Al_2O_3$ or $Y_2O_3$ with subsequent pyrolytic treatments at 1350 °C in an $N_2$ atmosphere was shown to lead to the formation of β-SiAlON ($Si_5AlON_7$) and $Y_4Si_2N_2O_7$, respectively.[16] Reactions between amorphous silicon carbonitride, $Al_2O_3$ or $Y_2O_3$, and amorphous $SiO_2$ contamination were presumed to cause the secondary phase formation. An increased weight loss at temperatures exceeding 1350 °C was explained by carbothermal reduction processes. More recently, Pashchanka et al.[17] reported the combination of a polysilazane with a porous $Al_2O_3$ template (PAOX) to yield ceramic nanowires and nanotubes after pyrolysis at temperatures up to 1100 °C in an Ar atmosphere. The composition of the nanoscaled products formed was found to be in the Si–O–(N)–C system. The presence of oxygen in the material was traced back to the involvement of –OH groups on the surface of the alumina substrate, present prior to coming into contact with the polymeric precursor.

Owing to the hydrolytically sensitive nature of polysilazanes, degradation of the polymer itself can even occur at room temperature in the presence of $H_2O$ or substances containing –OH groups, e.g. in a moist atmosphere, by hydrolysis/condensation processes, leading to the formation of Si–O–Si bonds.[18] The presence of adsorbed water and –OH groups on the surface of oxide ceramic filler particles, extensively reported in the literature,[19–21] is therefore presumed to be involved in the incorporation of oxygen in the polymeric matrix.

In the present work, the interactions between a poly(vinyl)silazane and the oxide ceramic filler components $Al_2O_3$ and $Y_2O_3$-stabilised $ZrO_2$ are investigated in order to explain an unexpected influence of the choice of filler on the composite's behaviour during processing, primarily concerning the compactibility during warm-pressing of the composite powders as well as the shrinkage during pyrolytic conversion. The focus is on alterations of the polysilazane during the coating of the filler powders and on the consequences of these alterations on secondary phase formation during the pyrolytic conversion in the temperature interval between 1000 °C and 1400 °C. Thereby possible phase compositions and resulting properties will be anticipated, this being crucial for the manufacturing of bulk polymer-derived ceramic materials.

## 2. Experimental

### 2.1. Starting materials

A liquid poly(vinyl)silazane (*KiON HTT 1800*, Clariant Advanced Materials GmbH, Germany) was used as the polymeric precursor. α-$Al_2O_3$ (*CT 3000 SG*, Almatis GmbH, Germany; mean particle size 0.5 μm) or 3 mol% $Y_2O_3$-stabilised $ZrO_2$ (*YZ01*, SEPR Saint-Gobain ZirPro, France; mean particle size 0.6 μm) were used alternatively as filler powders. The powders were pre-treated by attrition milling (Netzsch PE 075 with lining, stirrer and milling media made of $Al_2O_3$ or $ZrO_2$, respectively) in acetone for 2 h, dried, sieved (200 μm mesh), and stored at 110 °C. In this state, thermogravimetric analyses of the prepared filler powders were carried out in flowing Ar (50 ml $min^{-1}$) at temperatures up to 1000 °C (Netzsch STA 449 C Jupiter).

### 2.2. Production and characterization of composite mixtures

A polysilazane content of 40 vol.% in cross-linked state was chosen for the composite materials. This corresponds to a polysilazane content of 15.8 wt.% and 11.0 wt.%, respectively, for polysilazane/$Al_2O_3$ and polysilazane/$ZrO_2$ mixtures, taking into account the densities of the polysilazane ($\rho_p = 1.12$ g $cm^{-3}$) and the filler component ($\rho_f = 3.98$ g $cm^{-3}$ for $Al_2O_3$, $\rho_f = 6.05$ g $cm^{-3}$ for $ZrO_2$) obtained from the corresponding technical datasheets. The coating of the powders was carried out in an $N_2$ atmosphere at ambient temperatures by dispersing the filler powders in water-free cyclohexane (p.a., Merck), addition of the polysilazane and intensive stirring for 1 h. The solvent was removed in vacuo during continuous stirring. After complete drying, the composite mixture was sieved (63 μm mesh). At this point, NMR and FT-IR investigations of the composite mixtures and of the polysilazane (as shipped) were carried out. Solid-state nuclear magnetic resonance spectra were recorded with a Bruker spectrometer model AVANCE 300 equipped with a 4 mm broadband probe head ($^{13}C = 75.40$ MHz, $^{29}Si = 59.57$ MHz, $^{15}N = 30.39$ MHz with $^{15}NH_4Cl = 0$ ppm). All NMR measurements were conducted in HPDEC (high power decoupled) mode with a rotational speed of 4 kHz. The liquid polysilazane was investigated in non-rotating mode. FT-IR spectra were recorded with a Bruker Tensor 27 spectrometer with ATR MicroFocusing MVP-QL insert based on ZnSe optics.

### 2.3. Production and characterization of bulk specimens

The sieved composite mixture was warm-pressed at a pressure of 75 MPa at 200 °C for 4 h, in order to form cylindrical specimens with a diameter of 40 mm and a height of approximately 8 mm. The green density of the specimens was determined by the weight and the geometric dimensions. The theoretical green density was calculated according to the rule of mixtures.

Small cubical-shaped pieces of the warm-pressed specimens were used for dilatometry (Netzsch DIL 402 C) as well as thermogravimetry–mass spectrometry (TG–MS) investigations. For the latter, a Netzsch STA 449 C Jupiter simultaneous thermal analyser was used, coupled with a Netzsch QMS 403 C Aëolos mass spectrometer. Investigations were conducted in flowing $N_2$ (50 ml $min^{-1}$) with a heating rate of 5 K $min^{-1}$ applied to a maximum temperature of 1500 °C.

Dilatometric and thermogravimetric analyses with the same measurement parameters were also carried out for specimens consisting of 100% polysilazane, these acting as filler-free reference samples. In this case, the oxide ceramic filler powders were substituted with a pre-cured polysilazane (8 h at 200 °C) which had been ball-milled for 1 h and subsequently sieved (45 μm

Table 1
Heating profile during pyrolysis.

| Temperature region (°C) | Heating rate (K h$^{-1}$) |
|---|---|
| 20–300 | 300 |
| 300–500 | 180 |
| 500–800 | 60 |
| 800–1200 | 180 |
| 1200–1400 | 60 |

mesh). The pre-cured polysilazane powder was coated with liquid polysilazane and sieved as described in Section 2.2, with the resulting mixture warm-pressed as described above.

Pyrolytic treatments of the warm-pressed specimens were carried out in an $Al_2O_3$ tube furnace (Naber LHT8/R17) in flowing $N_2$ (0.35 l min$^{-1}$) at various temperatures between 1000 °C and 1400 °C with heating rates according to Table 1. The respective temperature of pyrolysis was held for 4 h before cooling with a rate of 180 K h$^{-1}$.

After pyrolysis, the apparent density of the specimens was determined by helium pycnometry (Quantachrome Ultrapycnometer 1000). The bulk density was determined by the Archimedes method. The theoretical density $\rho_{th}$ was calculated from Eq. (1), taking into account the density change in the polymer-derived ceramic component as well as the mass loss of the polymer component during pyrolysis:

$$\rho_{th} = \frac{1 - X_p \cdot M_p}{((M_p \cdot (1 - X_p))/(\rho_{p,pyro})) + ((1 - M_p)/(\rho_f))} \quad (1)$$

Here, $X_p$ is the mass loss fraction of the cross-linked polymer during pyrolysis, $M_p$ the weight content of the polymer in cross-linked state, $\rho_{p,pyro}$ the density of the polysilazane-derived component after pyrolysis, and $\rho_f$ the density of the filler component.

Values for $\rho_f$, $\rho_p$, and $\rho_{p,pyro}$ were obtained from the technical datasheets ($\rho_f$ = 3.98 g cm$^{-3}$ for $Al_2O_3$ or 6.05 g cm$^{-3}$ for $ZrO_2$, $\rho_{p,pyro}$ = 2.4 g cm$^{-3}$). The mass loss fraction $X_p$ of the cross-linked polysilazane component during pyrolysis was determined by thermogravimetric analysis of a pre-cured (200 °C for 8 h) sample in flowing $N_2$ (50 ml min$^{-1}$) at temperatures up to 1500 °C (Netzsch STA 449 C Jupiter). Linear shrinkage of the specimens during pyrolysis was deduced from the dimensional change. Phase investigations by XRD were carried out on a Philips X'Pert diffractometer. Changes in elemental composition of the samples were determined by X-ray fluorescence analysis (PANalytical Axios advanced). In order to evaluate the bulk microstructure, cross-sections of the pyrolysed samples were mounted in an epoxy resin, ground and polished, and investigated by secondary electron microscopy (SEM) on a FEI Quanta 200. Transmission electron microscopic (TEM) investigations were conducted on a FEI Tecnai F20 with FEG emitter after thinning of samples by focused ion beam (FIB).

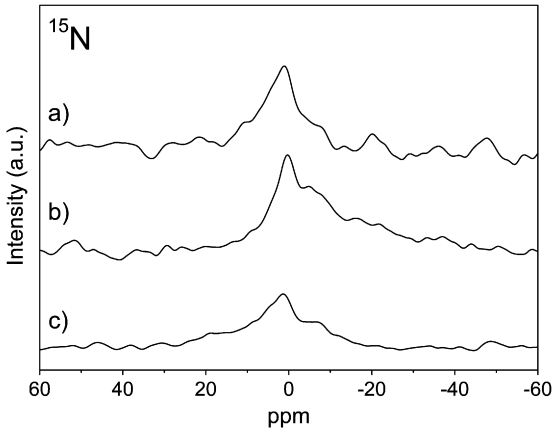


Fig. 1. $^{15}N$ solid-state NMR spectra for (a) polysilazane-coated $ZrO_2$ powder, (b) polysilazane-coated $Al_2O_3$ powder, and (c) polysilazane as-shipped.

## 3. Results and discussion

### 3.1. Polymer–filler interactions during composite powder preparation

By using attrition-milled powders, both fillers could be dispersed evenly in cyclohexane before the addition of the polysilazane to the mixture. After the removal of the solvent, differences in the coating behaviour of $Al_2O_3$ and $ZrO_2$ powders were observed. In the case of the polysilazane-coated $Al_2O_3$ filler, the dried composite mixture showed a tendency to form soft agglomerates, resulting in increased losses during the subsequent sieving process with sieving yields of 71–82%. In the case of polysilazane-coated $ZrO_2$ however, a solid, grindable mixture was obtained after removal of solvent, leading to improved sieving yields of 85–94%. A tendency to form hard agglomerate particles of size equal to the mesh size was observed.

In order to investigate the differences in coating behaviour, NMR and FT-IR studies were carried out on the composite mixtures after solvent removal, before the sieving process. No significant differences between samples can be seen in solid-state NMR investigations of $^{13}C$ and $^{29}Si$ (see Appendix A, Fig. A1 and Table A1). The results of the solid-state NMR studies of $^{15}N$ are shown in Fig. 1.

In the case of the $^{15}N$ NMR shifts are observed for the main peak: 1.38 ppm for the pure polysilazane, 0.96 ppm for the polysilazane–$ZrO_2$ mixture, 0.32 ppm for the polysilazane–$Al_2O_3$-mixture. In addition to the main peak, indications for a second peak are present in the shoulder region between 0 ppm and −10 ppm. For the polysilazane–$ZrO_2$ mixture, an intensity decrease (relative to the main peak intensity) in this region is visible when compared with the pure polysilazane as well as the polysilazane–$Al_2O_3$ mixture. This observation supports an assumption of accelerated degradation processes in the polysilazane–$ZrO_2$ mixture, possibly caused by reactions of Si–N groups.

Changes in the structure and composition of the polysilazane component after coating of the oxide ceramic filler particles are inferred from the FT-IR spectra. The results are given in Fig. 2, together with an assignment of the bands.[17,22] FT-IR spectra

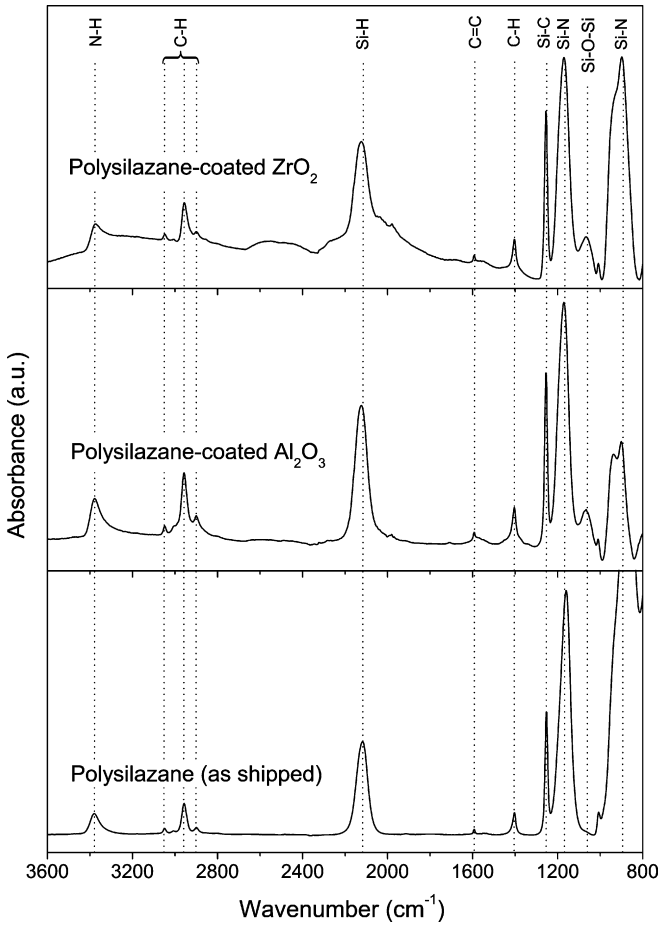


Fig. 2. FT-IR spectra and band assignments for polysilazane-coated $ZrO_2$ powder, polysilazane-coated $Al_2O_3$ powder and polysilazane as-shipped.

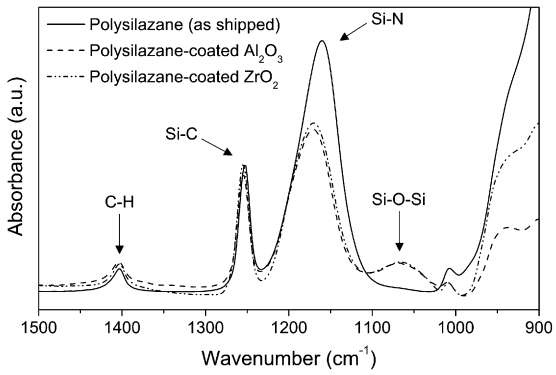


Fig. 3. IR absorption spectra of polysilazane as-shipped, polysilazane-coated $Al_2O_3$ powder and polysilazane-coated $ZrO_2$ powder (relative intensities normalised to the Si–C peak at 1255 $cm^{-1}$).

Table 2
Results of thermogravimetric analyses of attrition-milled filler powders, dried at 110 °C, before coating with polysilazane.

| Filler | $\Delta m/m_0$ | | | | |
|---|---|---|---|---|---|
| | at 200 °C | at 400 °C | at 600 °C | at 800 °C | at 1000 °C |
| $Al_2O_3$ | −0.11% | −0.35% | −0.50% | −0.54% | −0.55% |
| $ZrO_2$ | −0.08% | −0.63% | −0.82% | −0.88% | −0.90% |

obtained are generally similar all the systems investigated, with the exception of Si–O–Si functional groups becoming evident at 1033 $cm^{-1}$ in the polysilazane–filler-mixtures. Differences between spectra in the IR region below 1000 $cm^{-1}$ are influenced by IR absorption of the oxide ceramic filler particles, and are therefore omitted from further interpretation.

Compared to the intensities of non-hydrolysable Si–C functional groups at 1255 $cm^{-1}$, an appearance of Si–O–Si bands accompanied by a decrease in intensity of the Si–N bands in the polysilazane component is seen after coating of the filler particles (Fig. 3).

Since the coating process was carried out in an inert atmosphere and in a water-free solvent, the increase in intensity of Si–O–Si bands in the composite mixture can be attributed to the involvement of reactive groups on the particle-surfaces of the filler powders used. The presence of adsorbed $H_2O$ and –OH groups on particle surfaces at ambient conditions has been reported for many oxide ceramic materials, including $Al_2O_3$ [19,20] and $ZrO_2$.[21] In the present case, the formation of Si–O–Si linkages can be explained by hydrolysis/condensation processes of Si–N bonds in the polysilazane component in presence of $H_2O$. This is represented in the following simplified reaction:

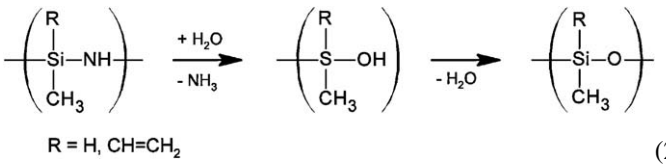


(2)

The hypothesis that reactive surface groups are involved is supported by thermogravimetric analyses of the attrition-milled filler powders before coating, which show the removal of volatile species during heating. Results of the TG investigations are given in Table 2. For both filler powders, a virtually complete removal of adsorbed volatile species is obtained at temperatures exceeding 800 °C. Storage of the filler powders at 110 °C is therefore insufficient for a full removal of $H_2O$ and –OH species from the powder surfaces.

### 3.2. Pyrolytic decomposition in presence of oxide fillers

Thermogravimetric analyses coupled with mass spectrometry were carried out in order to determine the interactions and reactivity between the polysilazane component and the filler powders during the pyrolytic conversion. In addition to the warm-pressed filler-containing specimens, a warm-pressed filler-free polysilazane was investigated as a reference sample. The results of the TG–MS studies are shown in Fig. 4. Since the studies were carried out in a flowing $N_2$ atmosphere, the species $N_2$ and CO (both $m/z = 28$) could not be investigated directly.

TG–MS investigations of the warm-pressed filler-free polysilazane sample (Fig. 4a) show a minor mass loss due to the

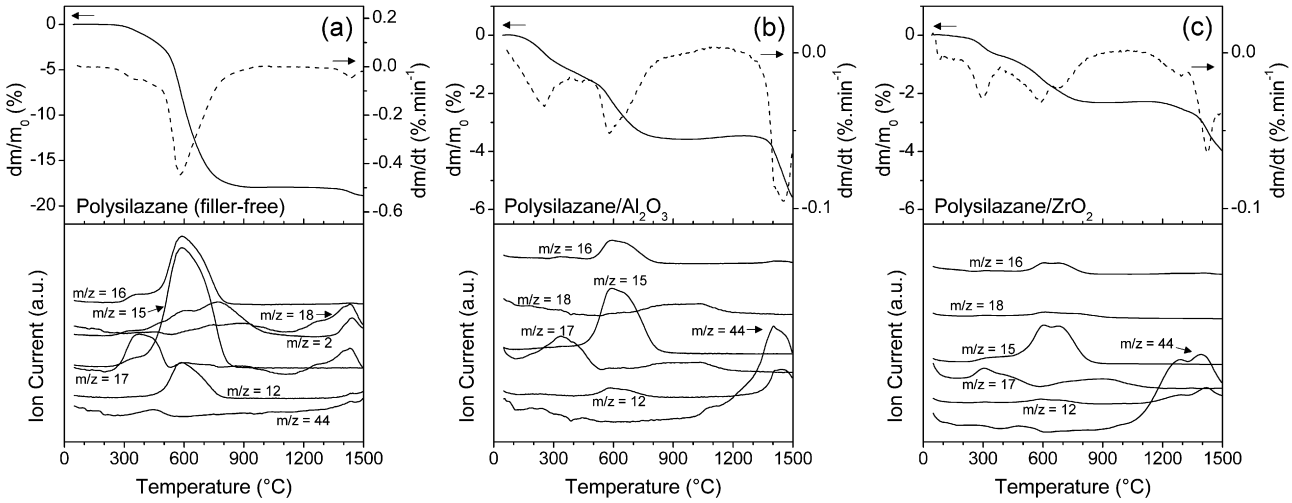


Fig. 4. TG–MS investigations in flowing $N_2$: mass change behaviour and evolving gases during heating of (a) warm-pressed filler-free polysilazane, (b) warm-pressed polysilazane/$Al_2O_3$ composite, and (c) warm-pressed polysilazane/$ZrO_2$ composite.

formation of $NH_3$ ($m/z = 17$) at temperatures between 300 °C and 500 °C, and a major mass loss at temperatures between 500 °C and 800 °C, accompanied by the evolution of hydrocarbon species such as methane ($m/z = 12$, 15, 16) as well as $H_2$ ($m/z = 2$). Further mass loss at temperatures exceeding 1200 °C can be attributed to the formation of $H_2O$ ($m/z = 17$, 18) in addition to minor amounts of $CO_2$ or SiO (both $m/z = 44$). From 1400 °C upwards, the evolution of $H_2$ ($m/z = 2$) can be detected. The heating ramp accounted for a mass loss of 18.9%, compared to an overall mass loss of 19.1% obtained after cooling. The results of the thermogravimetric investigation of the filler-free reference sample are in general agreement with the literature data for the pyrolysis of polysilazanes.[23,24]

In the case of the polysilazane/$Al_2O_3$ composite (Fig. 4b), three distinct mass loss regions can be observed. Up to a temperature of 400 °C, the mass change is caused primarily by the evolution of $NH_3$ ($m/z = 17$). Between 400 °C and 1300 °C, the results are similar to those for the filler-free polysilazane specimen, but with a correspondingly reduced mass loss due to the reduced polysilazane content. From 1300 °C upwards, a third mass loss region can be observed. Owing to the simultaneous detection of $m/z = 12$, the $m/z = 44$ peak can be attributed to $CO_2$, thereby ruling out the volatilisation of major amounts of SiO.

The behaviour of the polysilazane/$ZrO_2$ composite sample (Fig. 4c) differs from the polysilazane/$Al_2O_3$ sample mainly in the third mass loss region, from 1150 °C upwards. In contrast to the $Al_2O_3$-containing sample, a two-step mass loss can be observed, with mass change maxima at 1285 °C and 1425 °C, with corresponding peaks in $CO_2$ formation also observed.

The different behaviour of the $Al_2O_3$- and the $ZrO_2$-containing samples compared to the filler-free polysilazane, i.e. the increased mass loss in the temperature region up to 400 °C, can be explained by hydrolysis of Si-N bonds due to contaminant $H_2O$ on the surfaces of the filler powder particles. This in turn results in a shift of the $NH_3$ peak ($m/z = 17$) towards lower temperatures. In contrast, $NH_3$ evolution in the filler-free polysilazane can be explained by transamination processes during cross-linking.[23] Mass loss starting at 1150 °C and 1300 °C for polysilazane/$ZrO_2$ and polysilazane/$Al_2O_3$ composites, respectively, can be explained by carbothermal reduction processes, which have been reported for several combinations of polymer-derived ceramics with $Al_2O_3$.[10,16,17,25] $SiO_2$, originating from hydrolysis products during coating of the filler powders, is reduced by excess free carbon in the polysilazane-derived matrix component, yielding the volatile compounds SiO and CO:

$$SiO_2(s) + C(s) \rightarrow SiO(g) + CO(g) \quad (3)$$

Since a mass spectrometric detection of CO ($m/z = 28$) was not possible, due to the use of $N_2$ as purge gas, the presence of CO can be inferred from the simultaneous detection of C ($m/z = 12$) and $CO_2$ ($m/z = 44$). The absence of independent SiO peaks in the mass spectra can be explained by further reactions of SiO within the material or by premature condensation in the transfer capillary before reaching the mass detector.

The presence of carbothermic reduction processes at higher process temperatures resulted in a colour change of the pyrolysed specimens. After pyrolysis at 1000 °C and 1200 °C, the filler-containing specimens showed a dark grey appearance. When pyrolysed at 1400 °C, a brightening of the specimens due to the loss of free carbon was observed. This was true particularly for regions near the surface. The assumed loss of Si caused by the formation of volatile SiO was investigated by X-ray fluorescence analysis. Since this method is not adequate to determine the absolute composition of the specimens (due to the low sensitivity for lighter elements such as C and N), mass ratios Al/Si and Zr/Si were chosen for the two different fillers, in order to evaluate changes in elemental composition within the materials and at their surfaces. The results are given in Table 3.

Taking into account the relative Si content of the polysilazane precursor and the Al or Zr content of the respective filler powder, calculations yielded theoretical mass ratios of Al/Si = 6.5 and Zr/Si = 12.3 for the original composite powder mixtures. The calculated values are in good agreement with values determined by X-ray fluorescence analyses for pyrolysis temperatures of 1000 °C and 1200 °C. A pronounced loss of Si was found in surface near regions after pyrolysis at 1400 °C for

Table 3
Mass ratios of Al/Si and Zr/Si, in the bulk and at the surfaces of pyrolysed polysilazane/$Al_2O_3$ and polysilazane/$ZrO_2$ composites, respectively, as determined by X-ray fluorescence analysis.

| Material | Pyrolysis temperature (°C) | Mass ratio Me/Si (Me = Al or Zr) | |
|---|---|---|---|
| | | Bulk | Surface |
| Polysilazane/$Al_2O_3$ | 1000 | 6.6 | 6.4 |
| | 1200 | 6.9 | 7.1 |
| | 1400 | 7.3 | 18.6 |
| Polysilazane/$ZrO_2$ | 1000 | 12.0 | 10.9 |
| | 1200 | 12.3 | 14.3 |
| | 1400 | 11.8 | 119.4 |

both polysilazane/$Al_2O_3$ and polysilazane/$ZrO_2$ composites. In the case of the $ZrO_2$-filled sample, the Si content in the sample surface region fell by nearly 90%.

In addition to the reduction of $SiO_2$, carbothermal reduction of the oxide ceramic filler component itself is possible. Carbothermal reduction of $ZrO_2$ has been reported to take place at temperatures between 1200 °C and 1350 °C.[26,27] In case of $Al_2O_3$, carbothermal reduction to volatile $Al_2O$ and further reaction to AlN in presence of $N_2$ was reported to start at a temperature of 1350 °C[28]:

$$Al_2O_3(s) + 2C(s) \rightarrow Al_2O(g) + 2CO(g) \quad (4a)$$

$$Al_2O(g) + C(s) + N_2(g) \rightarrow 2AlN(s) + CO(g) \quad (4b)$$

### 3.3. Densification behaviour

After warm-pressing, the polysilazane/$Al_2O_3$ composites had a green density of $2.57 \pm 0.03\,g\,cm^{-3}$, corresponding to a relative green density of $90.6 \pm 0.9\%$. The warm-pressed polysilazane/$ZrO_2$ composites had a green density of $3.55 \pm 0.04\,g\,cm^{-3}$, the relative green density being $87.1 \pm 1.0\%$. The slightly impaired compressibility of the $ZrO_2$-containing samples was caused by the formation of hard agglomerates during the coating process as a result of the degradation of the polysilazane component. The applied pressure was insufficient to disintegrate the composite powder granules formed.

In order to calculate the theoretical densities of the pyrolysed samples according to Eq. (1), it was necessary to determine the mass loss fraction of the polysilazane component $X_p$. TG analysis of a pure polysilazane reference sample yielded a value of $X_p = 0.2$, corresponding to a ceramic yield of 80%. The density and porosity values of the pyrolysed samples are given in Table 4. In the case of polysilazane/$Al_2O_3$ composites, an increase in process temperature caused a decrease in bulk density, resulting in porosity values of up to 30%. Surprisingly, linear shrinkage of the specimens was not significantly affected by pyrolysis temperature in the observed temperature interval. In contrast, the polysilazane/$ZrO_2$ specimens exhibited a distinctly increased densification and shrinkage with rising process temperatures, yielding materials with minimum porosities of 6%.

Assuming that porosity in the prepared samples is present to a large extent in the form of open pores, apparent density determined by helium pycnometry should equal the theoretical density. A good agreement between calculated theoretical density and measured apparent density of the investigated specimens can be found for a pyrolysis temperature of 1000 °C. The general increase in apparent density with rising pyrolysis temperature can be explained by possible reactions between the polymer-derived matrix and the filler component. This also explains the deviation from calculated theoretical density values at higher process temperatures, since the formation of secondary phases has not been taken into account in the calculations.

The densification behaviour of the composites during pyrolysis was studied in more detail by dilatometric investigations (Fig. 5). In addition to the $Al_2O_3$- and $ZrO_2$-filled samples, a filler-free warm-pressed polysilazane sample was employed as a reference, in order to distinguish between shrinkage caused by the conversion of the polysilazane-derived matrix component and shrinkage influenced by interactions of the polysilazane component with the filler material.

The filler-free warm-pressed polysilazane (Fig. 5a) showed thermal expansion up to a temperature of 400 °C. Starting at 400 °C up to a temperature of 1200 °C, a steady shrinkage of the material with a maximum shrinkage rate at 600 °C occurred. The main dimensional change between 500 °C and 800 °C is caused by the polymer-to-ceramic conversion and coincides with the mass loss behaviour observed by TG–MS studies in the same temperature region. The dilatometric investigation of the polysilazane/$Al_2O_3$ composite (Fig. 5b) showed a weak shrinkage tendency during pyrolysis. In the temperature region below 800 °C, two local shrinkage maxima at 310 °C and 630 °C were

Table 4
Density, porosity, and shrinkage of the prepared specimens after pyrolytic conversion.

| Material | Calculated theoretical density $\rho_{th}$ ($g\,cm^{-3}$) | Pyrolysis temperature (°C) | Apparent density ($g\,cm^{-3}$) | Bulk density ($g\,cm^{-3}$) | Relative density[a] (%) | Total porosity[a] (%) | Linear shrinkage (%) |
|---|---|---|---|---|---|---|---|
| Polysilazane/$Al_2O_3$ | 3.665 | 1000 | 3.67 | 2.78 | 75.9 | 24.1 | 1.8 |
| | | 1200 | 3.72 | 2.70 | 73.7 | 26.3 | 1.8 |
| | | 1400 | 3.84 | 2.56 | 69.8 | 30.2 | 1.9 |
| Polysilazane/$ZrO_2$ | 5.323 | 1000 | 5.33 | 4.06 | 76.3 | 23.7 | 5.2 |
| | | 1200 | 5.43 | 4.20 | 78.9 | 21.1 | 6.7 |
| | | 1400 | 5.38 | 5.01 | 94.1 | 5.9 | 11.2 |

[a] With respect to the calculated theoretical density.

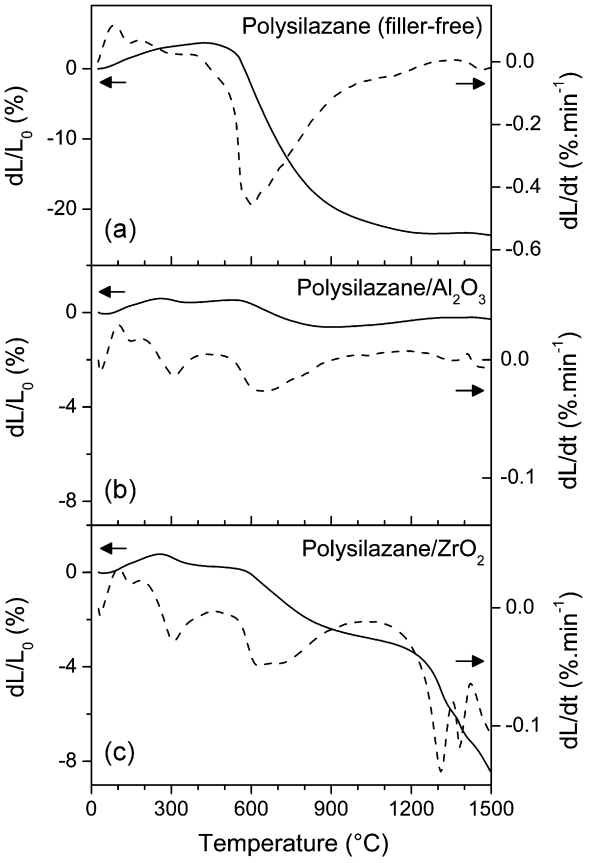


Fig. 5. Dilatometric investigations during heating of (a) warm-pressed filler-free polysilazane, (b) warm-pressed polysilazane/$Al_2O_3$ composite, and (c) warm-pressed polysilazane/$ZrO_2$ composite, carried out in flowing $N_2$.

observed. Between 800 °C and 1300 °C, the material exhibits no significant dimensional change. Further small shrinkage can be found above 1350 °C. The polysilazane/$ZrO_2$ composite (Fig. 5c) shows a qualitatively similar dimensional change behaviour up to a temperature of 1100 °C. However, the overall shrinkage is higher compared to the polysilazane/$Al_2O_3$ sample. Starting at 1150 °C, the material undergoes a strong densification, still continuing at the peak temperature of 1500 °C. Local shrinkage maxima were observed at 1310 °C and 1380 °C.

Through comparison with the filler-free reference sample, shrinkage in the temperature region between 400 °C and 800 °C can be attributed to intrinsic transformation processes in the polysilazane-derived matrix component. By contrast, shrinkage above 1150 °C is caused by interactions between the matrix and the filler component and/or sintering processes. In the case of polysilazane/$ZrO_2$ composites, the onset of shrinkage at 1200 °C is correlated with an increase in rate of mass loss in the same temperature region (see Fig. 4c). It can be assumed that shrinkage in this region is a result of reactions between constituents. Further information considering the formation of secondary phases and the development of the microstructure is necessary in order to interpret the results for mass change and densification presented here.

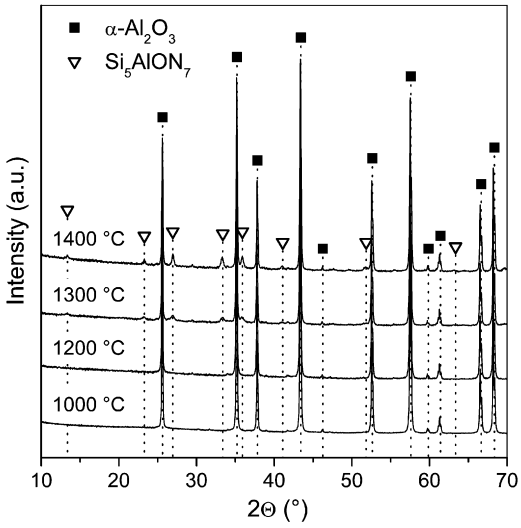


Fig. 6. X-ray diffraction patterns of a polysilazane/$Al_2O_3$ composite after pyrolysis at varying temperatures. (Reference data for $Al_2O_3$: PDF 81-2267; $Si_5AlON_7$: PDF 48-1615.)

### 3.4. Secondary phase formation and microstructure

The development of the crystalline phase composition of the polysilazane/oxide filler samples was investigated by X-ray diffraction analyses after pyrolysis at temperatures between 1000 °C and 1400 °C. In the case of polysilazane/$Al_2O_3$ specimens (Fig. 6), the filler component $Al_2O_3$ is the sole crystalline phase up to a temperature of 1200 °C. The presence of β-SiAlON ($Si_5AlON_7$) can be observed at 1300 °C, with increasing β-SiAlON content at 1400 °C.

In the case of $ZrO_2$-filled polysilazane, the formation of $ZrSiO_4$ was found (Fig. 7). Up to 1200 °C, the crystalline sample content is composed of $Y_2O_3$-stabilised $ZrO_2$, with small amounts of monoclinic $ZrO_2$ present. $ZrSiO_4$ can be identified after pyrolysis at temperatures of 1300 °C and higher. Crystalli-

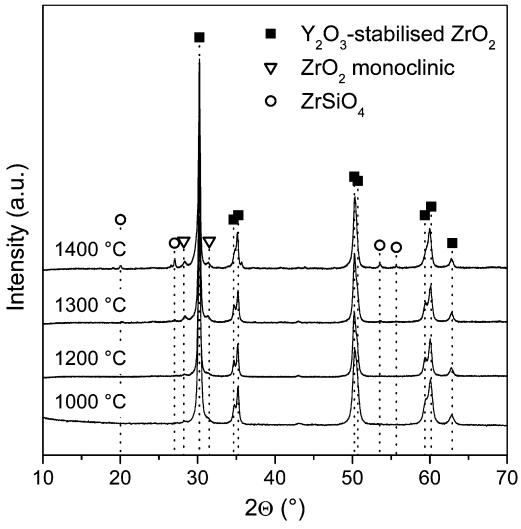


Fig. 7. X-ray diffraction patterns of a polysilazane/$ZrO_2$ composite after pyrolysis at varying temperatures. (Reference data for $Y_2O_3$-stabilised $ZrO_2$: PDF 83-0113; $ZrO_2$ monoclinic: PDF 37-1484; $ZrSiO_4$: PDF 83-1377.)

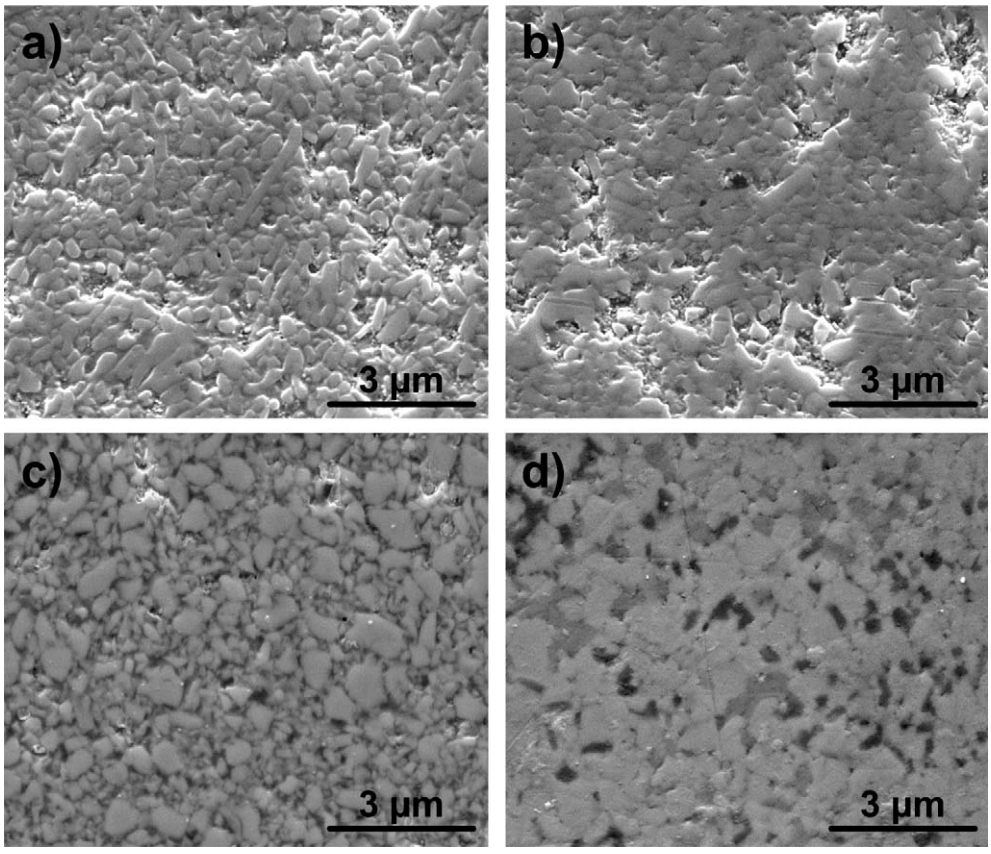


Fig. 8. SEM micrographs of polished cross-sections of specimens pyrolysed at varying temperatures: (a) polysilazane/$Al_2O_3$, 1000 °C; (b) polysilazane/$Al_2O_3$, 1400 °C; (c) polysilazane/$ZrO_2$, 1000 °C; (d) polysilazane/$ZrO_2$, 1400 °C.

sation products such as SiC or $Si_3N_4$, which would be expected to develop during the pyrolysis of a pure polysilazane at 1400 °C, were not found in the presence of $Al_2O_3$ or $ZrO_2$ fillers.

The formation of secondary phases such as $Si_5AlON_7$ and $ZrSiO_4$ is a result of the involvement of contaminant $SiO_2$. Oxygen contaminations are introduced into the system in the form of Si–O–Si linkages during the coating of the filler powders, these being transformed to $SiO_2$ during pyrolysis. In order to yield $Si_5AlON_7$, $SiO_2$ in the amorphous matrix component can react with $Al_2O_3$ or with AlN obtained by carbothermal reduction in the presence of $N_2$, as described in Eqs. (4a) and (4b). The formation of β-SiAlON from $Al_2O_3$, $SiO_2$, and C in $N_2$ atmospheres at 1350 °C, following the intermediate formation of mullite ($3Al_2O_3{\cdot}2SiO_2$) between 1200 °C and 1400 °C, has been reported in the literature.[29] Interestingly, no mullite crystallisation was observed in the polysilazane/$Al_2O_3$ samples investigated. The process yielding $Si_5AlON_7$ can be summarised by the following reaction equation:

$$Al_2O_3 + 10SiO_2 + 21C + 7N_2 \rightarrow 2Si_5AlON_7 + 21CO \quad (5)$$

Thermogravimetric analyses of polysilazane/$Al_2O_3$ composites confirm the assumption of this overall reaction, since the evolution of large amounts of CO was found at temperatures above 1350 °C (Fig. 4b).

The observed formation of $ZrSiO_4$ in polysilazane/$ZrO_2$ composites can be explained by the following reaction equation:

$$ZrO_2 + SiO_2 \rightarrow ZrSiO_4 \quad (6)$$

The reaction between $Y_2O_3$-stabilised $ZrO_2$ and $SiO_2$ has been reported to take place at temperatures as low as 1230 °C.[30] $ZrSiO_4$ formation can therefore be attributed to the dilatometrically investigated dimensional change of polysilazane/$ZrO_2$ composites at temperatures exceeding 1200 °C with a maximum shrinkage peak at 1310 °C (Fig. 5c).

SEM images of the samples' microstructure after pyrolytic treatment are shown in Fig. 8. In case of the $Al_2O_3$-filled specimens (Fig. 8a and b), no significant densification was achieved by an increase in pyrolysis temperature. Areas with high polymer content and thus increased porosity are visible, independent of process temperature. In case of the polysilazane/$ZrO_2$ composites, significant differences in microstructure can be observed after variation of pyrolysis conditions (Fig. 8c and d). Increased shrinkage of the polysilazane/$ZrO_2$ composite after pyrolytic treatment at 1400 °C results in a densified material (Fig. 8d), which is in good accordance to the low porosity values observed.

In order to further examine the effects of the described reactions between the polysilazane-derived matrix phase and the respective filler particles on the material's microstructure

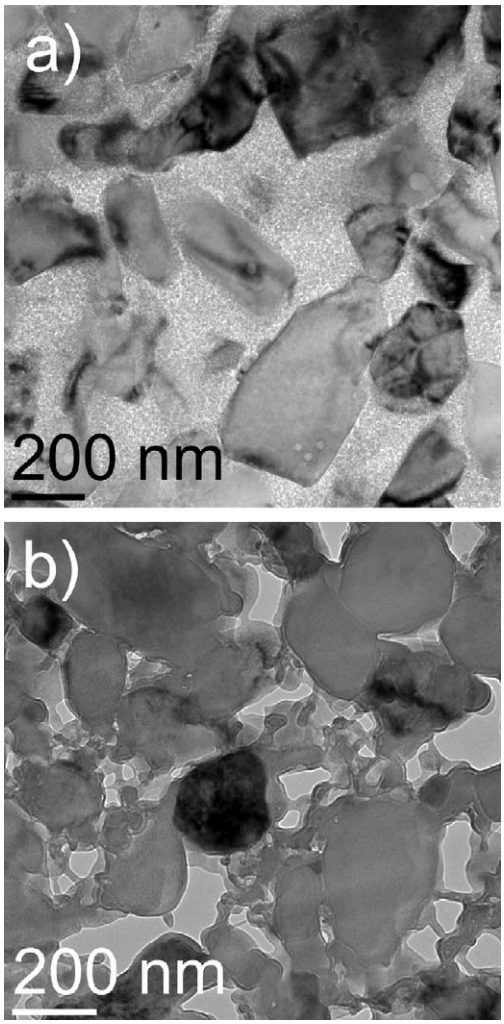


Fig. 9. TEM micrographs of the bulk structure of a polysilazane/$Al_2O_3$ composite after pyrolysis at (a) 1000 °C and (b) 1400 °C.

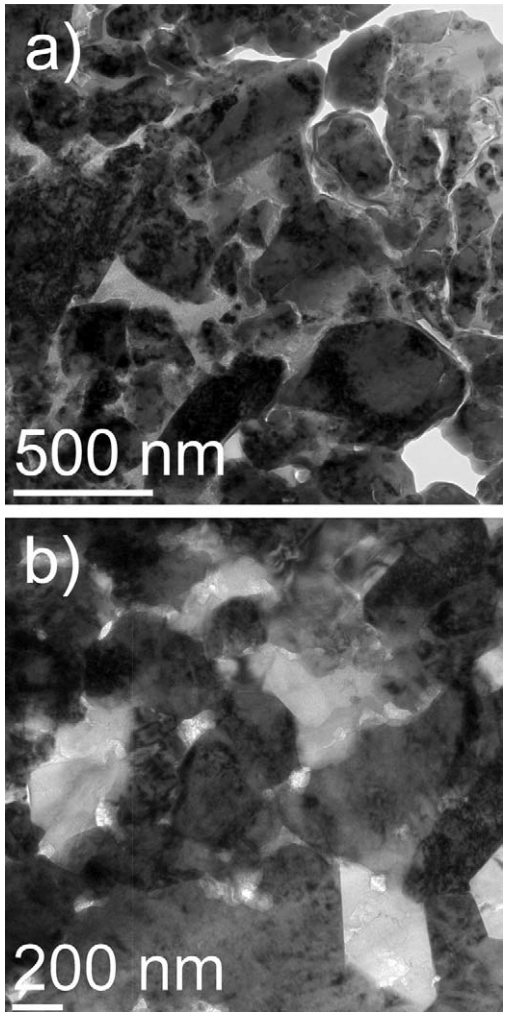


Fig. 10. TEM micrographs of the bulk structure of a polysilazane/$ZrO_2$ composite after pyrolysis at (a) 1000 °C and (b) 1400 °C.

and its behaviour during pyrolysis, TEM analyses were conducted. TEM micrographs of polysilazane/$Al_2O_3$ specimens after pyrolysis at 1000 °C and 1400 °C are shown in Fig. 9. $Al_2O_3$ filler particles are densely embedded in the amorphous polysilazane-derived matrix component after pyrolytic treatment at 1000 °C (Fig. 9a). In contrast, large amounts of residual porosity are visible after pyrolysis at 1400 °C (Fig. 9b). Unreacted remains of the $Al_2O_3$ particles are interconnected by reaction products of polysilazane-derived matrix and filler.

As presented in Eq. (5), the formation of $Si_5AlON_7$ is accompanied by the evolution of large quantities of gaseous reaction products such as CO. Furthermore, volatile SiO is formed by carbothermal reduction of $SiO_2$. Both processes are responsible for the formation of secondary porosity in the material. The formation of porosity thus effectively counteracts shrinkage, which is in good agreement with the results of the dilatometric investigations, yielding an effective linear shrinkage of only 2% after pyrolysis at 1400 °C.

The $ZrO_2$-filled polysilazane exhibits a significantly different evolution of microstructure during pyrolysis (Fig. 10). After pyrolytic treatment at 1000 °C, primary $ZrO_2$ particles are incorporated in the amorphous polysilazane-derived matrix, as for the polysilazane/$Al_2O_3$ sample (Fig. 10a). However, after pyrolysis at 1400 °C, a densification of the former material is visible (Fig. 10b).

The formation of neck structures between particles is an indication for sintering processes at this temperature, leading to further densification. As a result, linear shrinkage of nearly 12% was observed after pyrolysis at 1400 °C. In contrast to $Al_2O_3$-filled polysilazane specimens, no significant formation of secondary porosity is visible.

EDS analyses of the $ZrO_2$-filled polysilazane after pyrolysis at 1400 °C show that $ZrSiO_4$ is formed at the interface between the $ZrO_2$ filler particles and the oxygen-containing amorphous polysilazane-derived matrix component (Fig. 11). $ZrSiO_4$ formation can therefore be held responsible for the comparably higher shrinkage of polysilazane/$ZrO_2$ composites compared to $Al_2O_3$-filled polysilazane at temperatures between 1200 °C and 1400 °C.

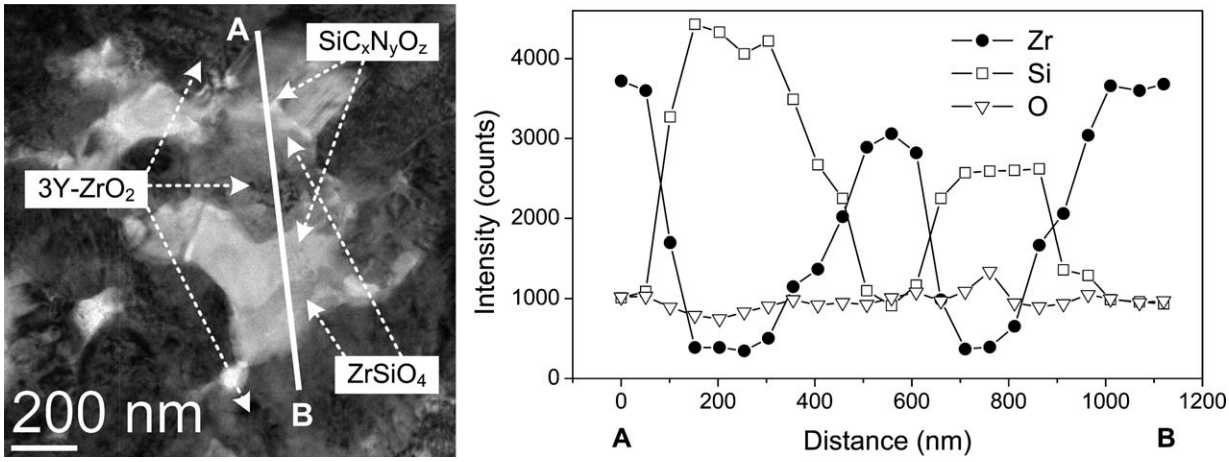


Fig. 11. TEM micrograph of a polysilazane/$ZrO_2$ composite after pyrolysis at 1400 °C with labelled constituents (left) and corresponding elemental distributions of Zr, Si, and O (right), as determined by EDS line scan.

## 4. Conclusions

The interactions between a polysilazane and the oxide ceramic filler powders $Al_2O_3$ and $Y_2O_3$-stabilised $ZrO_2$ have been investigated. Structural and compositional monitoring was carried out during the initial coating of the filler powders with the polymer, as well as during pyrolytic conversion of the warm-pressed polysilazane/filler composites in flowing $N_2$.

The presence of adsorbed species such as $H_2O$ or –OH groups on the surfaces of the filler powders prior to use was found to influence the processing behaviour of the polysilazane/filler composites significantly, as well as the composition of the final ceramic products. The incorporation of oxygen into the pre-ceramic polymer matrix was shown to take place through the formation of Si–O–Si groups. During pyrolysis, these groups were transformed to $SiO_2$ which in turn participated in further reactions, depending on the ceramic filler. The presence of oxide fillers resulted in the formation of secondary reaction products in the form of $Si_5AlON_7$ for $Al_2O_3$ and $ZrSiO_4$ for $ZrO_2$, respectively, at temperatures $\geq$1300 °C. In spite of comparable mass loss characteristics, significant differences in the densification behaviour were observed. Depending on the reaction mechanism of secondary phase formation, the quantity of volatile reaction products such as CO or SiO, and the sintering tendency of the materials generated, linear shrinkage of the resulting materials was shown to vary between 2% for $Al_2O_3$ filler and 12% for $ZrO_2$ filler after pyrolysis at 1400 °C. TEM studies indicated the differences in shrinkage to be caused by the formation of large amounts of secondary porosity in $Al_2O_3$-filled specimens as opposed to ongoing sintering processes for $ZrO_2$-filled samples in the temperature region between 1200 °C and 1400 °C.

Based on the results of this study, targeted alterations in the surface chemistry of filler powders would be a promising possibility for further controlling the pyrolytic conversion of polymer-derived ceramics with particulate fillers. Following this approach, the reactivity between polymer-derived matrix and filler could be controlled by systematical thermal or chemical pre-treatment of filler powders, with a corresponding impact on the composition of the final ceramic product. The resulting changes in porosity and microstructure can be expected to influence material properties significantly, in particular mechanical properties such as strength.

## Acknowledgments

The authors would like to thank Dr. Erich Halwax and Dr. Christian Gierl (both at the Institute of Chemical Technologies and Analytics, Vienna University of Technology) for assistance in XRD and TG–MS measurements. Furthermore, we acknowledge Dr. Hannes Zbiral for performing RFA analyses. TEM investigations were carried out by Dr. Johannes Bernardi using facilities at the University Service Centre for Transmission Electron Microscopy, Vienna University of Technology. Prof. Noel Thomas of Koblenz University of Applied Sciences is gratefully acknowledged for linguistic advice.

## Appendix A. Supplementary data

Supplementary data associated with this article can be found, in the online version, at doi:10.1016/j.jeurceramsoc.2011.07.015.

## References

1. Greil P. Near net shape manufacturing of polymer derived ceramics. *J Eur Ceram Soc* 1998;**18**(13):1905–14.
2. Riedel R, Kleebe HJ, Schönfelder H, Aldinger F. A covalent micro/nano-composite resistant to high-temperature oxidation. *Nature* 1995;**374**:526–8.
3. An L, Riedel R, Konetschny C, Kleebe HJ, Raj R. Newtonian viscosity of amorphous silicon carbonitride at high temperature. *J Am Ceram Soc* 1998;**81**(5):1349–52.
4. Rice RW. Ceramics from polymer pyrolysis, opportunities and needs – a materials perspective. *Am Ceram Soc Bull* 1983;**62**(8):889–92.
5. Seyferth D, Wiseman GH. High-yield synthesis of $Si_3N_4$/SiC ceramic materials by pyrolysis of a novel polyorganosilazane. *J Am Ceram Soc* 1984;**67**(7):C132–3.
6. Riedel R, Strecker K, Petzow G. In situ polysilane-derived silicon carbide particulates dispersed in silicon nitride composite. *J Am Ceram Soc* 1989;**72**(11):2071–7.

7. Kraus T, Günthner M, Krenkel W, Motz G. cBN particle filled SiCN precursor coatings. *Adv Appl Ceram* 2009;**108**(8):476–82.
8. Borsa CE, Jones NMR, Brook RJ, Todd RI. Influence of processing on the microstructural development and flexure strength of $Al_2O_3$/SiC nanocomposites. *J Eur Ceram Soc* 1997;**17**(6):865–72.
9. Sternitzke M, Derby B, Brook RJ. Alumina/silicon carbide nanocomposites by hybrid polymer/powder processing: microstructures and mechanical properties. *J Am Ceram Soc* 1998;**81**(1):41–8.
10. Galusek D, Sedláček J, Riedel R. $Al_2O_3$–SiC composites prepared by warm pressing and sintering of an organosilicon polymer-coated alumina powder. *J Eur Ceram Soc* 2007;**27**(6):2385–92.
11. Brahmandam S, Raj R. Novel composites constituted from hafnia and a polymer-derived ceramic as an interface: phase for severe ultrahigh temperature applications. *J Am Ceram Soc* 2007;**90**(10):3171–6.
12. Riedel R, Mera G, Hauser R, Klonczynski A. Silicon-based polymer-derived ceramics: synthesis properties and applications – a review. *J Ceram Soc Jpn* 2006;**114**(6):425–44.
13. Greil P. Active-filler-controlled pyrolysis of preceramic polymers. *J Am Ceram Soc* 1995;**78**(4):835–48.
14. Seyferth D, Bryson N, Workman DP, Sobon CA. Preceramic polymers as "reagents" in the preparation of ceramics. *J Am Ceram Soc* 1991;**74**(10):2687–9.
15. Colombo P, Mera G, Riedel R, Sorarù GD. Polymer-derived ceramics: 40 years of research and innovation in advanced ceramics. *J Am Ceram Soc* 2010;**93**(7):1805–37.
16. Lee SH. Processing of carbon fiber reinforced composites with particulate-filled precursor-derived Si–C–N matrix phases. Ph.D. Thesis. University of Stuttgart; 2004.
17. Pashchanka M, Engstler J, Schneider JJ, Siozios V, Fasel C, Hauser R, et al. Polymer-derived SiOC nanotubes and nanorods via a template approach. *Eur J Inorg Chem* 2009;**23**:3496–506.
18. Bauer F, Decker U, Dierdorf A, Ernst H, Heller R, Liebe H, et al. Preparation of moisture curable polysilazane coatings: Part I. Elucidation of low temperature curing kinetics by FT-IR spectroscopy. *Prog Org Coat* 2005;**53**:183–90.
19. Knözinger H. Hydrogen bonds in systems of adsorbed molecules. In: Schuster P, Zundel G, Sandorfy C, editors. *The hydrogen bond*, vol. 3. Amsterdam: North-Holland; 1976. p. 1263–364.
20. Al-Abadleh HA, Grassian VH. FT-IR study of water adsorption on aluminum oxide surfaces. *Langmuir* 2003;**19**:341–7.
21. Agron PA, Fuller EL, Holmes HF. IR studies of water sorption on $ZrO_2$ polymorphs. I. *J Colloid Interface Sci* 1975;**52**(3):553–61.
22. Schrader B. Vibrational spectroscopy of different classes and states of compounds. In: Schrader B, editor. *Infrared and Raman spectroscopy: methods and applications*. Weinheim: Wiley-VCH; 1995. p. 188–222.
23. Bahloul D, Pereira M, Goursat P, Choong Kwet Yive NS, Corriu RJP. Preparation of silicon carbonitrides from an organosilicon polymer: I. Thermal decomposition of the cross-linked polysilazane. *J Am Ceram Soc* 1993;**76**(5):1156–62.
24. Haluschka C, Kleebe HJ, Franke R, Riedel R. Silicon carbonitride ceramics derived from polysilazanes: Part I. Investigation of compositional and structural properties. *J Eur Ceram Soc* 2000;**20**:1355–64.
25. Galusek D, Klement R, Sedláček J, Balog M, Fasel C, Zhang J, et al. $Al_2O_3$–SiC composites prepared by infiltration of pre-sintered alumina with a poly(allyl)carbosilane. *J Eur Ceram Soc* 2011;**31**: 111–9.
26. Gruner W, Stolle S, Wetzig K. Formation of $CO_x$ species during the carbothermal reduction of oxides of Zr, Si, Ti, Cr, W, and Mo. *Int J Refract Met Hard Mater* 2000;**18**:137–45.
27. Maitre A, Lefort P. Solid state reaction of zirconia with carbon. *Solid State Ionics* 1997;**104**:109–22.
28. Chen HK, Lin CI, Lee C. Kinetics of the reduction of carbon/alumina powder mixture in flowing nitrogen stream. *J Am Ceram Soc* 1994;**77**(7):1753–6.
29. Sopicka-Lizer M, Terpstra RA, Metselaar R. Carbothermal production of β′-SiAlON from alumina, silica and carbon mixture. *J Mater Sci* 1995;**30**:6363–9.
30. Kaiser A, Lobert M, Telle R. Thermal stability of zircon ($ZrSiO_4$). *J Eur Ceram Soc* 2008;**28**:2199–211.